パルス変調マイクロ波励起の水蒸気プラズマを用いた高速フォトレジスト膜除去法の開発

著者	相澤 洸
著者別表示	AIZAWA Takeshi
雑誌名	博士論文要旨Abstract 要約Outline
学位授与番号	13301甲第5588号
学位名	博士（工学）
学位授与年月日	2022-09-26
URL	http://hdl.handle.net/2297/00068843

甲（Kou）
様式　４．（Form 4）

学　位　論　文　概　要
Dissertation Summary

学位請求論文（Dissertation）
題名（Title）パルス変調マイクロ波励起の水蒸気プラズマを用いた高速フォトレジスト膜除去法の開発
Development of High-Speed Photoresist Film Ashing Process using Pulse Modulated Microwave-Excited Water Vapor Plasma

専攻（Division）：電子情報科学専攻
学籍番号（Student ID Number）：1724042006
氏名（Name）：相澤　洸
主任指導教員氏名（Chief supervisor）：石島　達夫

学位論文概要（Dissertation Summary）

1. Introduction

Chemical treatment and oxygen plasma treatment have been commonly used for photoresist removal in semiconductor processes for a long time. In recent years, in these circumstances, there is a demand for environmentally friendly and high-speed photoresist removal method. We are developing an environmentally friendly photoresist removal method using water vapor as the source gas and we intended to practical use of water-vapor plasma ashing method for a minimal-fab system. The objective of this work was fundamental investigation of water-vapor plasma and to improve its performance. In order to adapt WPA for practical process, I have developed the enlargement of the plasma and improvement of its uniformity, and have realized a high-speed ashing rate for ion-implanted photoresist films.

2. Fundamental investigation of water-vapor plasma ashing (WPA) method

2.1. Effects of square wave modulation of microwave power

Microwave power affects the size, density, and probability of ignition of the plasma. However, when the high microwave power is injected, thermally-equilibrium plasma will generate. Therefore, input microwave power is operated with a square wave modulation in order to reduce energy-transfer duration among particles. Observations of high-speed camera revealed that a large plasma was generated when the on-time was more than 3 ms. It was found the modulation frequency (f_{mod}) of 100 Hz and 30% duty factor (DF) in the frequency range from 100 Hz to 50 kHz.

2.2. Measurement of radiation intensity distribution by OES

Figure 1(a) presents a distribution of radiation intensity from the plasma. The center of the antenna surface is set as (x, y, z)=(0, 0, 0). The x-axis dependence of the radiation intensity decreased gradually as increasing x for all active species as shown in Fig.1(b). However, the intensity OH radical was slightly higher at x=1 mm than at x=0 mm. Figure 1(c) depicts z-axis dependence of the radiation intensity. The radiation intensities of all species except OH were highest at z=1 mm, whereas the radiation intensity of OH was highest at z=2 mm. The difference between the radiation intensity distribution of OH and the others (H_α, H_β, and O) is attributed to the threshold energies in the dissociation reaction of water molecules. The dissociation reaction in eq. (1) occurs when water collides with

electrons with energy greater than 9.15 eV. However, when the electron energy is higher than 17.19 eV, the dissociation reaction of eq. (2) occurs. In other words, at high electron energies, OH is produced in the ground state, not in the excited state. For this reason, H_α and O were strong, whereas OH (A-X) was weak near the antenna surface.

$$H_2O + e\ (E_{min} > 9.15\ eV) \rightarrow OH^*\ (A) + H\ (n = 1) \quad (1)$$

$$H_2O + e\ (E_{min} > 17.19\ eV) \rightarrow OH\ (X) + H^*\ (n = 3) \quad (2)$$

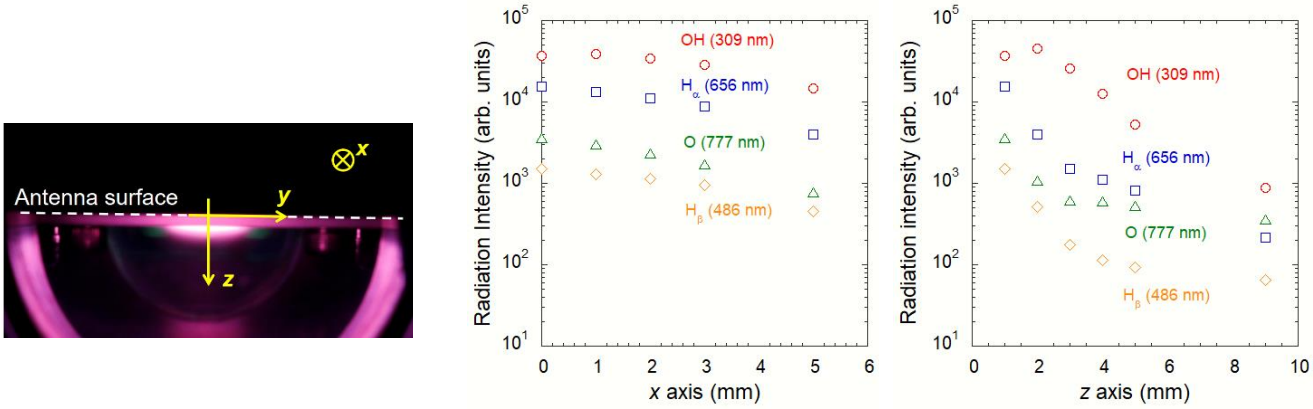

(a) Detail of xyz axis (b) (x, y, z)=(x, 0, 1) (c) (x, y, z)=(0, 0, z)

Fig. 1. Emission intensity distribution of OH, H_a, H_b, and O at P_{peak}=133 W, DF=30%, f_{mod}=100 Hz.

3. Enlarged plasma and improved ashing rate uniformity for a half-inch wafer

3.1. Investigation of novel antenna structures by electromagnetic field simulation

The slot antenna structure was modified to generate uniform plasma and thereby improve the ashing rate uniformity. The antenna structure was designed using commercially available electromagnetic wave simulation software: CST Microwave Studio©. Figure 2 presents a simplified model based on which the simulation was performed. The antenna surface on the chamber side was set as z = 0 mm. The electric field distribution was evaluated at z = 6.0 mm. Figure 3 portrays the antenna structure in this simulation model. This simulation investigated a slot antenna with a single slit (Fig. 3(a)), an H-shaped antenna with rectangular space at both ends of the slit (Fig. 3(b)), a double H-shaped (DH) antenna (Fig. 3(c)), and a double U-shaped (DU) antenna (Fig. 3(d)). Figure 4 presents simulation results of the electric field distribution at z = 6.0 mm. The electric field distribution of the slot antenna in Fig. 4(a) is elliptical. This distribution matches well with the appearance of the plasma light emission and the ashing shape of the photoresist in an earlier study. The H-shaped antenna presented in Fig. 4(b), the electric field distribution is circular instead of an elliptical shape. The double H-shaped antenna presented in Fig. 4(c), the electric field distribution is divided into top and bottom for the 0.5 inch wafer size. For the double U-shaped antenna presented in Fig. 4(d), the electric field distribution was much greater over the 0.5 inch wafer size.

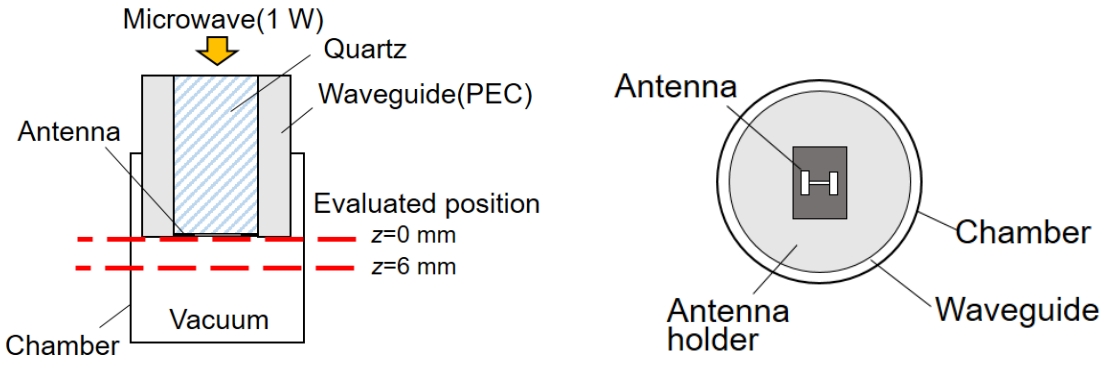

(a) Side view (b) Bottom view

Fig. 2. Simulation model and evaluation position of electric field intensity.

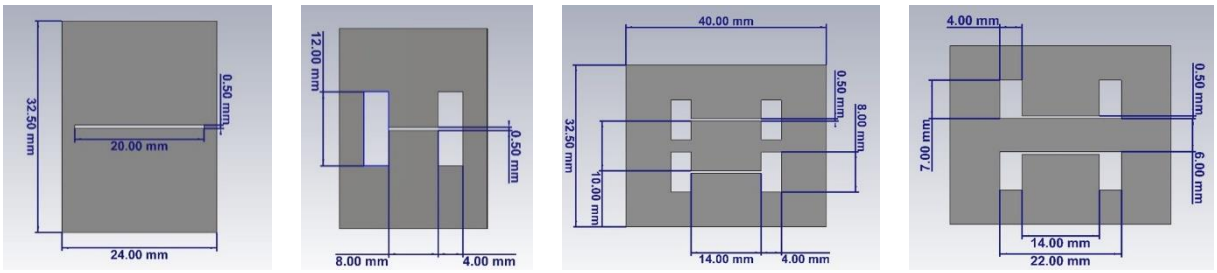

(a) Slot antenna (b) H-shaped (c) DH-shaped (d) DU-shaped

Fig. 3. Simulated antenna structure.

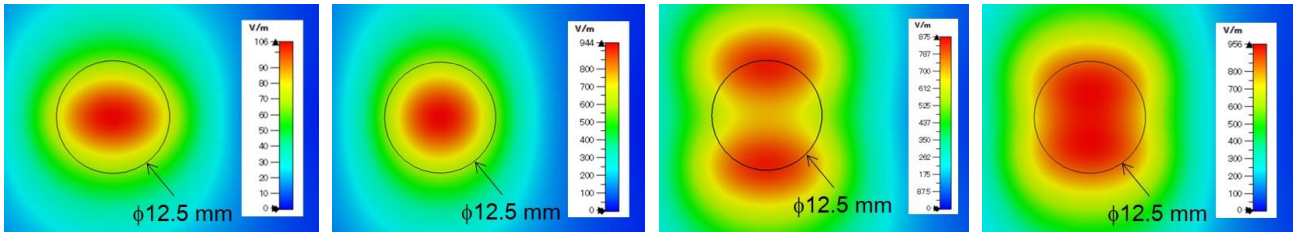

(a) Slot antenna (b) H-shaped (c) DH-shaped (d) DU-shaped

Fig. 4. Electric field intensity distribution at z=6 mm for each antenna.

3.2. Ashing rate distribution for four types of antennas

Fig. 5 shows the ashing rate distribution found for each antenna. The maximum value of the color map is the same as the maximum value of the ashing rate. For the slot antenna, the photoresist was removed with an elliptical shape under influence by the elliptical plasma shape. However, with the H-shaped antenna, the photoresist was removed with a circular shape influenced by the circular plasma shape. These distribution results are similar to the electric field distribution. In the double H-shaped antenna, the photoresist was removed with a distribution of high ashing rates at the top and bottom. By the double U-shaped antenna, the photoresist was removed more uniformly over the entire wafer surface than other antennas, indicating improved uniformity. Moreover, the ashing rate was higher than other antennas.

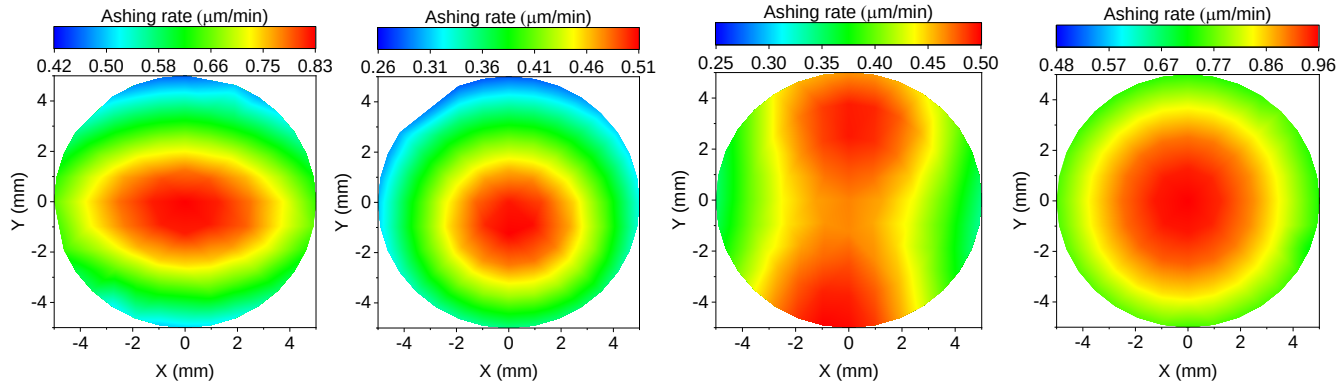

(a) Slot antenna (b) H-shaped (c) DH-shaped (d) DU-shaped

Fig. 5. Ashing rate distribution for each antenna at d=6.3 mm, f_{mod}=100 Hz, P_{peak}=200 W, DF=30%.

4. Water-vapor plasma ashing of high-dose ion-implanted photoresist.

4.1. Applying rf bias voltage to the substrate

In the case of the implanted photoresist with high doses ions is heated, then the photoresist will rupture. This phenomenon, called popping, leads to much residue on a wafer. Therefore, it is necessary to develop a low-temperature and high-speed ashing removal method for implanted photoresist with high dose ions. For this study, we introduced an rf bias voltage application on a substrate holder in the WPA to achieve a high ashing rate at a low substrate temperature.

Figure 6 presents emission images of the water vapor plasma taken using a digital camera. The plasma was observed through the quartz window on the side of the chamber. For the case without rf bias voltage, plasma generated by the microwave was observed near the antenna. However, for the case with rf bias voltage, plasma was generated simultaneously both near the antenna and near the wafer surface by the application of high voltage due to rf bias. Figure 7(a) and (b) shows the photoresist on the wafer after water vapor plasma ashing. In the condition without rf bias voltage, the photoresist was removed only slightly. In contrast, in the condition with rf bias voltage, the photoresist removal proceeded. The surface of the photoresist film was smooth without clear holes, suggesting popping was negligibly suppressed. The shape of the photoresist removal was circular. The removal speed near the wafer center appeared to be the highest.

Figure 7(c) portrays the photoresist thickness after ashing, as measured by the step profiler. The average film thickness in the radial direction is shown with the wafer center at 0 mm. Error bars represent the maximum and minimum thicknesses. The initial thicknesses of the photoresist film were 0.57 μm. For the case without bias voltage, results show little change from the initial film thickness. For the case with rf bias voltage, results show that the photoresist implanted high-doses of ions can be removed, despite the short irradiation time. The averaged ashing rate for r = 0.5 mm was estimated as 1.0 μm/min.

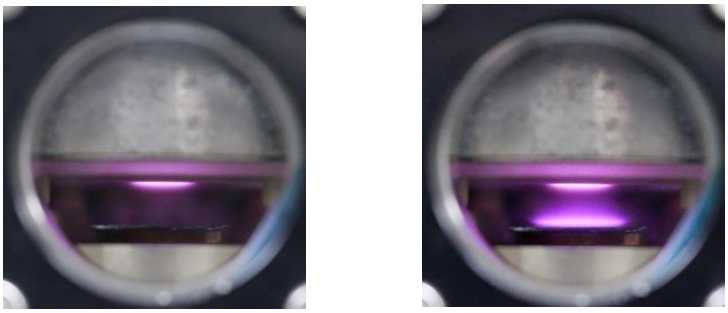

(a) Without bias voltage (b) With bias voltage at V_{pp}=1 kV

Fig. 6. Emission images of the plasma at f_{mod}=100 Hz, P_{peak}=200 W, DF=30%.

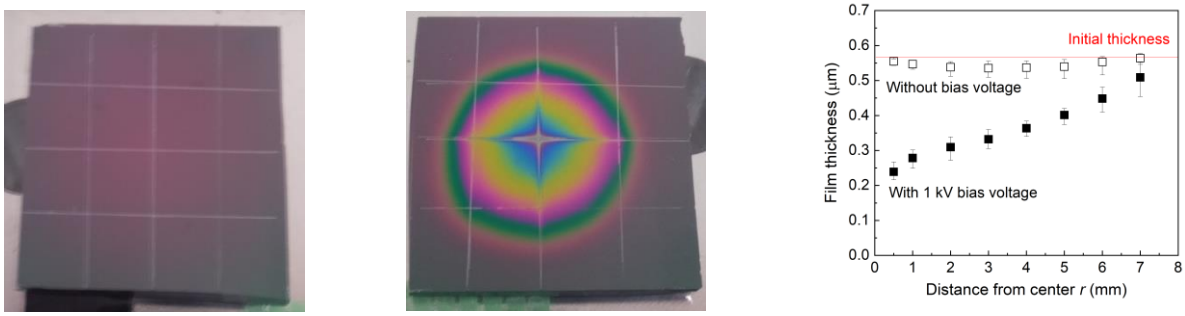

(a) Without bias voltage (b) With bias voltage at V_{pp}=1 kV (c) Photoresist film thickness

Fig. 7. Images and remaining photoresist film thickness of the ion-implanted photoresist with boron with an implantation dose of 1×10^{16} atoms/cm^2 after 20 s ashing at f_{mod}=100 Hz, P_{peak}=200 W, DF=30%.

5. Conclusion

In this thesis, the author proposed, (i) the DU-shaped antenna structure for improved ashing rate uniformity for half-inch wafer, (ii) apply rf bias voltage to the substrate holder for both popping suppression and high-speed photoresist removal. The ashing rate of 1 μm/min or higher could be obtained for high-dose ion-implanted photoresist without causing popping with the application of 1 kV rf bias voltage.